USE OF ACOUSTIC CAMERAS IN DREDGING RESEARCH

D.L. Young[1], B.C. McFall[2], T.L. Welp[3], and D.D. Dickerson[4]

ABSTRACT

The US Army Corps of Engineers (USACE) Dredging Operations Environmental Research (DOER) program addresses the science, engineering, and technology concerning dredging and managing approximately 150 million m^3 of sediment annually in support of navigation infrastructure, channels, ports, and harbors in the United States. The DOER Sediment/Dredging Processes and Environmental Resource Protection focus areas are currently conducting research and development activities that involve the use of a 3.0 MHz high resolution/high-definition imaging sonar (acoustic camera). These activities consist of two components: (1) a laboratory experiment to quantify the settling velocity of inertial negatively-buoyant particles suspended in the water column using acoustic camera images, with the long-term objective of adapting this technology to quantify velocity fields in turbid environments by tracking suspended non-inertial particles and (2) a field deployment in which an acoustic camera, bolted to a pan/tilt rotator assembly with two degrees of viewing freedom, was mounted on the turning gland of the dragarm of the USACE hopper dredge ESSAYONS to investigate its ability to operate in the dynamic and turbid environment of an operating dredge. This paper describes these two research initiatives utilizing sonar imaging technology. During lab trials the acoustic camera was able to quantify the terminal fall velocities of particles (with a size range of $0.5 - 5\ mm$) to within 1% of the theoretical terminal fall velocity for all particles, as well as qualitatively reproduce the expected settling behavior of the particles tested. In the field, the camera proved substantially more capable than concurrently deployed optical cameras in monitoring the operational efficiency of turtle tickler chains (an alternative turtle protection engineering control), as well as the interaction of the draghead and turtle deflector with the sediment, in the turbid environment of an operational dredge.

Keywords: Dredging, acoustic camera.

INTRODUCTION

As the dredging industry continues to stay at the forefront of technological innovation, state-of-the-art technologies and methods are developed, tested, and used to maintain navigable waterways in the most efficient, safe, and environmentally-friendly way practicable. To that end, the U.S. Army Corps of Engineers (USACE), with funding through the Dredging Operations and Environmental Research (DOER) program, is investigating the application of high-resolution acoustic cameras to monitor the highly turbid environments in the vicinity of dredging operations. Acoustic cameras, or imaging sonars, are small multi-beam active sonars that are able to "see" in turbid environments. They transmit sound pulses into the region of interest and use the returning sound to reconstruct a digital image. The range to the scattering object is determined by the time elapsed between the emission of the sound pulse and the return of the sound scattered by the object (Urick 1983). The direction to the scattering object relative to the camera position is determined by "beamforming" (or "spatial filtering") – using the observed lag between adjacent transducers observing the same sound returning to the transducer array to estimate the direction (Van Veen and Buckley 1988). The frequency of the sound pulses transmitted from the acoustic camera partially dictates the operating range of the acoustic camera and the resolution of the reconstructed image. In general, lower frequency (longer wavelength) sound pulses can penetrate further into the water column than higher frequency pulses (shorter wavelength), albeit with reduced spatial resolution in the resulting image.

[1] Research Engineer, U.S. Army Engineer Research and Development Center, 3909 Halls Ferry Road, Vicksburg, Mississippi 39180, USA, T: 601-634-5311, Email: David.L.Young@usace.army.mil.

[2] Research Engineer, U.S. Army Engineer Research and Development Center, 3909 Halls Ferry Road, Vicksburg, Mississippi 39180, USA, T: 601-634-6015, Email: Brian.C.McFall@usace.army.mil.

[3] Research Engineer, U.S. Army Engineer Research and Development Center, 3909 Halls Ferry Road, Vicksburg, Mississippi 39180, USA, T: 601-634-2083, Email: Timothy.L.Welp@usace.army.mil.

[4] Research Engineer, U.S. Army Engineer Research and Development Center, 3909 Halls Ferry Road, Vicksburg, Mississippi 39180, USA, T: 601-634-3772, Email: Dena.D.Dickerson@usace.army.mil.

These cameras may offer the potential to monitor dredging operations, study entrainment risk, and quantify two dimensional velocity fields by particles suspended in the water column. Researchers from the USACE Engineer Research and Development (ERDC) deployed a high-resolution acoustic camera in the laboratory to track the settling of inertial particles and estimate their fall velocity as a first step towards tracking non-inertial particles as required for estimating flow velocity. The camera was also deployed in the field - mounted to the dragarm of the USACE hopper dredge ESSAYONS - to investigate its ability to operate in the dynamic turbid environment of an operating dredge.

LABORATORY EXPERIMENT DESIGN

The laboratory experiments to investigate the acoustic camera's ability to track inertial particles and estimate fall velocity were conducted in December of 2016 at ERDC in Vicksburg, MS. The acoustic camera was placed on its side at mid-depth in a stainless steel tank (cross section - $3\ m\ \times 3\ m$), filled with tap water to a depth of $70\ cm$. The perimeter of the tank was blanketed with horse-hair to minimize acoustic reflection from the tank walls. The acoustic camera used in the experiment was a Sound Metrics ARIS 3000 Explorer Imaging Sonar (see Figure 1 - Sound Metrics Corp., Bellevue, Washington), with an operating frequency of $3\ MHz$. The camera was equipped with a 1° concentrator lens, which reduces the spreading angle of the acoustic camera to 1° (from a standard spreading angle of 14°) without altering the operating frequency of the camera. This focuses the acoustic energy into a narrower volume, increasing the resolution of the images and allowing smaller particles to be observed.

Figure 1. Picture of a Sound Metrics ARIS 3000 Imaging Sonar (Sound Metrics Corp., Bellevue, Washington). Re-printed from www.soundmetrics.com with permission.

With the camera in this configuration, the measurement volume resembles a very thick plane that stretches from the bottom of the tank to the water surface. A wave dampening device was placed on the water surface to both minimize surface disturbances as well as easily locate the free-surface position in the acoustic camera images. Figure 2 depicts the experimental setup including the position of the measurement volume.

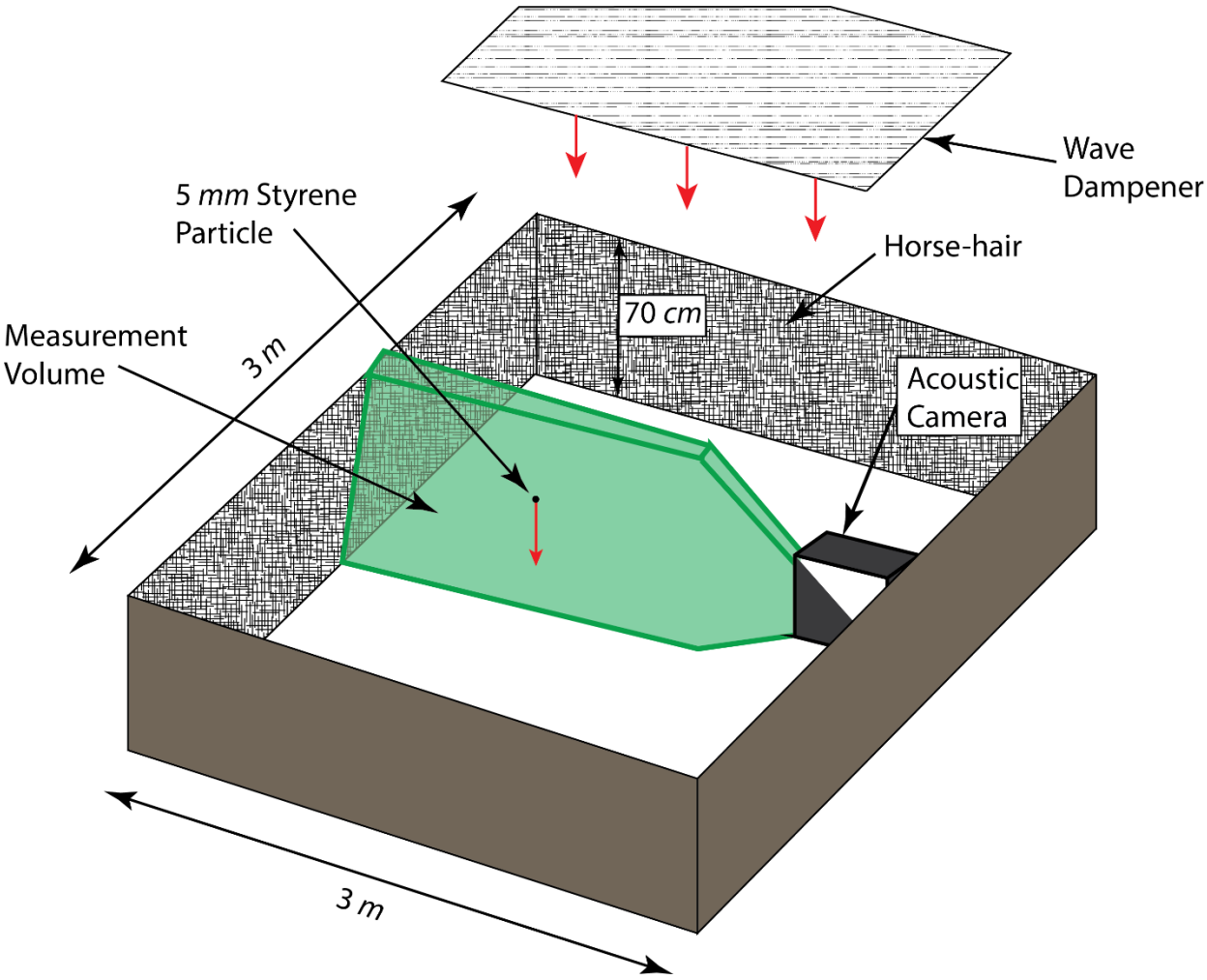

Figure 2. Diagram of the fall velocity laboratory experiment.

The fall velocities of three different particles were tested in this manner: a 5 mm (Poly)styrene sphere, a 1 mm Cellulose Acetate sphere, and a 0.5 mm Polymethyl Methacrylate (PMMA) sphere. The diameter and density of these particles are found in Table 1.

Table 1. Properties of the three particle types.

Particle Type	**d_s range** (mm)	**Assumed d_s** (mm)	**ρ_s range** (kg/m^3)	**Assumed ρ_s** (kg/m^3)
0.5 *mm* PMMA	0.425 – 0.5	0.465	1186.5	1186.5
1 *mm* Cellulose Acetate	1	1	1280	1280
5 *mm* Styrene	5	5	1040 - 1060	1050

Each particle was released just below the water surface with zero initial velocity and the motion of the particles was observed with the acoustic camera (see Figure 2) at 15 fps.

LABORATORY DATA ANALYSIS

The raw data returned by this acoustic camera consists of the intensity of the returned sound at a series of 600 bins, equidistantly spaced within each camera beam. The acoustic camera used in this experiment possesses 128 beams, each emitted at a slightly different angle such that collectively they span the entire width of the viewing window (or height, if the camera is on its side as in Figure 2). Using simple trigonometry, the angle of each individual beam relative to the camera axis, and the distance from the acoustic camera to the sample bin, it is possible to reconstruct a Cartesian image from the raw polar coordinate data. This procedure is performed using a custom Matlab (Mathworks, Inc., Natick, Massachusetts) script written with guidance from Sound Metrics. As a consequence of the polar-to-Cartesian conversion, the "resolution" of the Cartesian image must be manually specified rather than directly determined by the pixel resolution of the imaging sensor as is the case for an image acquired with a digital camera.

The raw Cartesian images are filtered with a separate custom Matlab script, which subtracts the average pixel intensity across time from each pixel, then sets to zero any pixels that fall below a specified threshold intensity. The filtered images are then written to audio video interleaved (.avi) files. A sub-window of a pre- and post-filter image is shown in Figure 3. Note that the subtraction of the time-averaged pixel intensity removes any stationary objects from the image, and the imposition of a lower bound on the pixel intensity returns only the brighter pixels (i.e., the particle centroid).

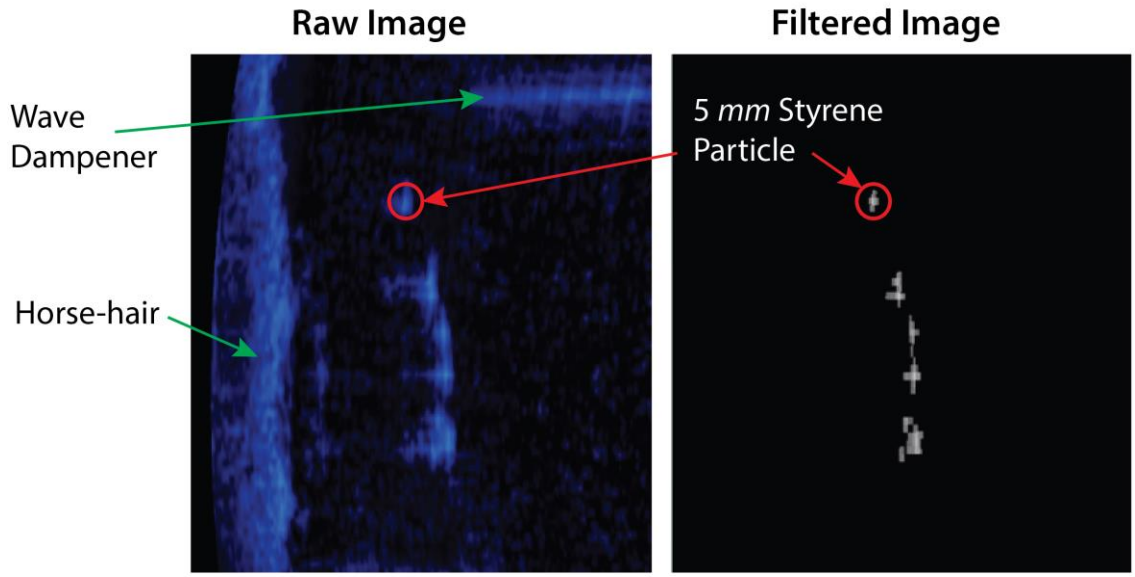

Figure 3. Sub-window of an acoustic camera image pre- and post-filtering.

The .avi movies of the filtered acoustic camera images are loaded into DLTdv5, a Matlab-based particle tracking routine developed by Ty Hedrick at UNC Chapel Hill (Hedrick 2008). DLTdv5 supports manual particle tracking, but also possesses an auto-tracking routine. The auto-tracking routine uses a localized Kalman filter in conjunction with a Gaussian peak detection scheme to estimate the position of the particle in the subsequent frame based on the particle trajectory in the previous frames, then searches the adjacent pixels for the particle centroid. Figure 4 shows the position of a tracked particle at three frames of an .avi file.

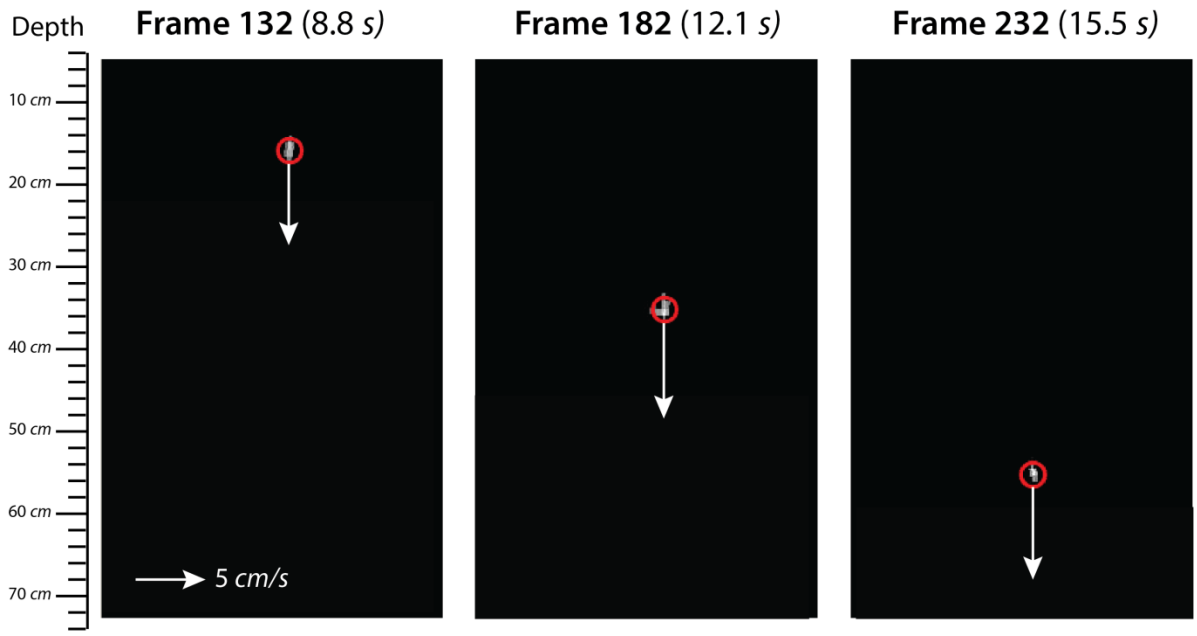

Figure 4. Depth and measured velocity (white arrow length) of a tracked 5 mm Styrene particle at 50 frame intervals. The time corresponds to the time elapsed from the beginning of the .avi file.

The tracking procedure returns comma separated value (.csv) files of the particles' locations within each frame of the .avi file (in pixels). These particle trajectories are loaded into a third custom Matlab script for analysis. The pixel coordinates are converted to physical position in mm using the pre-determined conversion factor specified in the polar-to-Cartesian image conversion Matlab script. The particle positions are smoothed using a moving median filter with a span of 20 particle positions, then the particle fall velocity is estimated via first order central differencing of the vertical particle positions (a forward and backwards differencing scheme are used for the first and last particle positions, respectively). The velocities themselves are smoothed using a moving average filter with a span of 30 particle velocities to return the instantaneous velocity measurements.

PARTICLE SETTLING VELOCITY THEORY

As per Munson et al. (2002), the terminal fall velocity for a sphere is reached when the negative buoyancy of the sphere is exactly balanced by the drag exerted on the sphere by the fluid. Under these conditions, the fall velocity for the sphere can be calculated as:

$$V = \sqrt{\frac{4gd_s}{3C_d}\left(\frac{\rho_s-\rho}{\rho}\right)} \tag{1}$$

where V is the (terminal) fall velocity, g is the acceleration due to gravity, d_s is the sphere diameter, C_d is the drag coefficient for the sphere, ρ_s is the density of the sphere, and ρ is the density of the fluid. The drag coefficient for a sphere is a function of the Reynolds number (Re), a dimensionless parameter that accounts for the relative importance of inertial forces relative to viscous forces in a fluid flow (Kundu and Cohen 2008). The Reynold number can be calculated from:

$$Re = \frac{Vd_s}{\nu} \tag{2}$$

where, ν is the kinematic viscosity of the fluid and, as in the previous equation, V and d_s are the terminal fall velocity and the sphere diameter, respectively. For $Re \lesssim 1$, the drag coefficient of a smooth sphere can be directly calculated

as $C_d = {}^{24}/_{Re}$. For $Re > 1$, there is no exact analytical expression for the functional dependence of the drag coefficient on the Reynolds number. However, the drag coefficient can still be estimated from a plot is generated by aggregating the results from a variety of experiments over a wide range of Reynolds numbers (e.g., Figure 9.21 in Munson et al. 2002 or Figure 10.23 in Kundu and Cohen 2008).

The fall velocity asymptotically approaches the terminal fall velocity as the sphere accelerates, corresponding with the drag on the sphere increasing towards equilibrium with the negative buoyancy. The relative rate at which the forces on the spherical particle approach this balance (and the particle approaches terminal fall velocity) is characterized by a non-dimensional parameter called the Stokes number (Stk). The Stokes number is the ratio of the characteristic response time of the particle, $\tau_p \cong d_s^2 \frac{(\rho_s - \rho)}{18\mu}$ (Tropea et al. 2007), to the characteristic time of the flow (τ_f) – in this case the approximate duration required for a particle to settle to the bed ($\tau_f \cong {}^{h}/_{V}$). In these expressions μ is the dynamic viscosity of the fluid and h is the water depth. As in previous equations, d_s is the sphere diameter, ρ_s is the density of the sphere, ρ is the density of the fluid, and V is the terminal fall velocity. The Stokes number can therefore be estimated from Equation 3.

$$Stk \cong \frac{d_s^2 V(\rho_s - \rho)}{18\mu h} \tag{3}$$

A lower Stokes number indicates that the particle will approach equilibrium more rapidly.

LABORATORY RESULTS AND DISCUSSION

The instantaneous fall velocities measurements of the three particles measured with the acoustic camera are plotted as a function of depth in Figure 5. The terminal fall velocity is estimated to be the average velocity of the deepest one-third of the velocity measurements, corresponding to those measurements made at depths greater than $\sim 56\ cm$. The measured terminal fall velocity for the three particles based on this criterion is shown with a color-coded dashed line in Figure 5. This is an admittedly heuristic approach, but does appear (at least in Figure 5) to allow sufficient time for all three particles to approach their respective maximum observed velocities. The theoretical terminal fall velocity for each of the three particles is calculated from Equation 1 (using information from Table 1 and Table 3), displayed in Figure 5 as a color-coded solid line, and tabulated in Table 2.

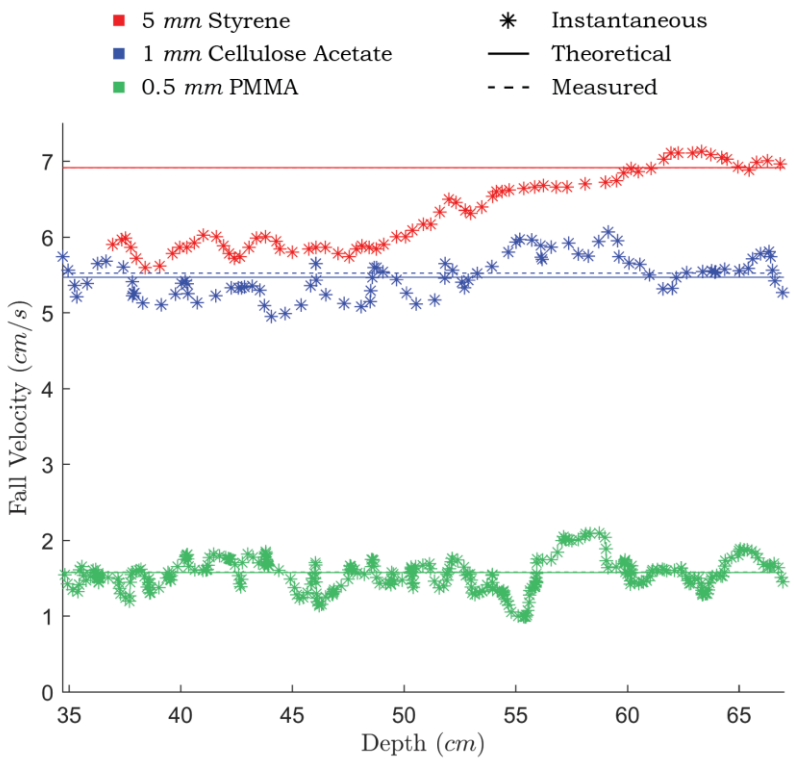

Figure 5. Measured instantaneous velocity as a function of depth, estimated terminal fall velocity, and theoretical terminal fall velocity for the three particles. Note that the dashed lines depicting the measured fall velocities for the 5 *mm* Styrene (red) and 0.5 *mm* PMMA particles (green) are obscured by the near perfect agreement with the theoretical fall velocities (solid lines).

Table 2. Comparison of the measured terminal fall velocity and the theoretical terminal fall velocity for the three particles.

Particle Type	**Measured Fall Velocity** (cm/s)	**Theoretical Fall Velocity** (cm/s)	**Error** (mm/s)	**% Error**
0.5 *mm* PMMA	1.58	1.57	+ 0.06	+ 0.40
1 *mm* Cellulose Acetate	5.53	5.47	+ 0.55	+ 1.00
5 *mm* Styrene	6.91	6.91	- 0.01	- 0.02

Table 3. Non-dimensional parameters for the three particle types (Reynolds number - Re and Stokes number - Stk) as well as the estimated drag coefficients (based on the calculated Reynolds number and Fig. 9.21 in Munson et al. 2002).

Particle Type	Re	C_d	Stk
0.5 *mm* PMMA	6.9	4.60	49.3
1 *mm* Cellulose Acetate	52.5	1.23	1208
5 *mm* Styrene	328.5	0.70	6176

The drag coefficient input in Equation 1 is a function of the Reynolds number. The Reynolds number for the three particles is calculated from Equation 2, using the measured fall velocity as the characteristic velocity, and displayed in Table 3. The drag coefficient is then estimated from a plot of the functional dependence of the drag coefficient on the Reynolds number for a smooth sphere (Fig. 9.21 in Munson et al. 2002) and tabulated in Table 3. It is worth noting that this plot is always displayed on log-log axes.

Figure 5 and Table 2 show excellent agreement between the measured and theoretical fall velocities for all three particles. The measured and theoretical fall velocities of the 5 mm Styrene and 0.5 mm PMMA particles are in such outstanding agreement that the measured fall velocity dashed lines are entirely obscured by the theoretical fall velocity solid lines. As indicated in Table 2, the percent error between the measured and terminal fall velocities (the error between the two values as a percentage of the theoretical terminal velocity) is ≤ 1 % for all three particle types.

Several other features are immediately apparent from Figure 5 and the results in Table 2. Perhaps the most obvious is that the maximum observed fall velocity for the 5 mm Styrene particle is greater than both the 1 mm Cellulose Acetate and the 0.5 mm PMMA particles. This despite the fact that Cellulose Acetate and PMMA are substantially more dense than Styrene (1280 $^{kg}/_{m^3}$ and 1186.5 $^{kg}/_{m^3}$ vs. 1050 $^{kg}/_{m^3}$ – see Table 1). This is because the *importance* of the negative buoyancy force relative to the drag force increases with increasing particle diameter (Tropea et al. 2007), and the 5 mm Styrene particle is substantially larger than either the 1 mm Cellulose Acetate or 0.5 mm PMMA particles.

Additionally, Figure 5 shows that the 0.5 mm PMMA particle (and to a lesser extent the 1 mm Cellulose Acetate particle) have effectively reached their terminal velocities by the time they settle into the measurement volume at a depth of $\sim 35\ cm$. In contrast, the 5 mm Styrene particle continues to accelerate to a depth of $\sim 60\ cm$. This observation is unsurprising given the Stokes numbers for the three particles (see Table 3). The Stokes number of the 5 mm Styrene particle is more than five times larger than that of the 1 mm Cellulose Acetate particle, and nearly 125 times larger than that of the 0.5 mm PMMA particle.

These results indicate acoustic cameras may be a valuable tool for examining the behavior of inertial particles suspended in a fluid flow. The qualitative behavior of the three particles (see Figure 5) agrees well with the expected behavior, specifically the relative terminal fall speeds among the three particle types, as well as the rate at which the particles approach the maximum observed fall velocity. Moreover, the quantitative measurements of the terminal fall velocity agreed extremely well with accepted theory – the percent error between the measured and theoretical terminal fall velocities is ≤ 1 % for all three particle types (see Table 2). This suggests that acoustic cameras are able to make accurate quantitative measurements of particle motion in a suspended flow for particles 0.5 mm in diameter and larger.

FIELD DEPLOYMENT

An acoustic camera was mounted on the ESSAYONS's dragarm as part of a preliminary field study to evaluate turtle tickler chains (TTC) as a potential replacement for draghead turtle deflectors. A further objective of this deployment was to investigate the feasibility of using an acoustic camera for monitoring equipment near or on a draghead during actual dredging operations. Incidental take of sea turtles is a potential risk during hopper dredging throughout sea turtle coastal habitats. Over the past 15 years the international dredging community has incorporated sea turtle protection methods developed by the USACE into some of their hopper dredging projects when practicable. However, differences in environmental conditions for international projects may preclude the use of some sea turtle protection methods typically used during US dredging projects. Therefore, alternative protection measures have been employed during these projects. One such method is a curtain of chains – turtle tickler chains (TTC) - hanging off the dragarm pipe ahead of the draghead. These TTC are designed to be dragged along the seafloor and startle or motivate a turtle on or near the seafloor to move away from the oncoming draghead – thus avoiding a turtle take by the draghead. The TTC technique is inspired by the similarly-named method employed by the fishing industry to motivate organisms to move off the seafloor ahead of fishing nets. Various versions of these TTC have been deployed during hopper projects outside the US including Gorgon, Western Australia and São João da Barra, Brazil. Although the TTC have been employed on these projects, their effectiveness in protecting sea turtles has not been documented.

Therefore, the primary objectives of the field deployment were to demonstrate the feasibility of using TTC and to document the technology's operational performance during a hopper dredging project in Kalaeloa Barber's Point Harbor, Oahu, Hawaii. The primary TTC performance metrics to be monitored included assurances that: (1) the

individual chains hung relatively straight in water column and maintained quasi-steady spacing between individual chain lengths, (2) the chains did not entangle - thereby creating a drowning risk to turtles, and (3) the chains maintained contact with the seafloor ahead of the draghead while it was on bottom. However, the field deployment did not quantify the effectiveness of the TTC in reducing incidental take of sea turtles. The operational performance of the TTC was monitored using an acoustic camera in conjunction with two other types of conventional underwater camera systems (GoPro cameras and a high definition video camera system) over a short period of time. Whereas, quantifying the effectiveness of the TTC in reducing incidental take of sea turtles would require a substantially longer term study and an endangered species observer to monitor all data collected. The sea turtle protection equipment (including draghead turtle deflector and TTC) and protocols, along with the endangered species monitoring requirements used during the Five Hawaii Commercial Harbors Maintenance Dredging Project, can be found in the project Biological Opinion (National Marine Fisheries Service 2016).

FIELD DEPLOYMENT EQUIPMENT

Figure 5 shows the draghead turtle deflector and TTC mounted on ESSAYONS's port dragarm. A Sound Metrics ARIS 3000 Explorer Imaging Sonar (Sound Metrics Corp., Bellevue, Washington – see Figure 1) with a pan/tilt rotator assembly and two degrees of viewing freedom was mounted on a custom frame and bolted to the aft flange of the dragarm turning gland. The pan and tilt rotator assembly for the acoustic camera, in conjunction with the mount location on the dragarm, allowed the camera to be remotely operated and view either the TTC or the draghead (see Figure 6). The camera's power/communications cable was attached to the dragarm pipe and frame, and run down into a below deck space (the boatswain's locker) where it was connected to the video monitoring and data recording computer. A GoPro camera (GoPro, Inc., San Mateo, California) and the high definition video recording camera were mounted just forward of the TTC on the dragarm gimbal. Another GoPro was mounted on the underside of turning gland immediately aft and over the TTC array.

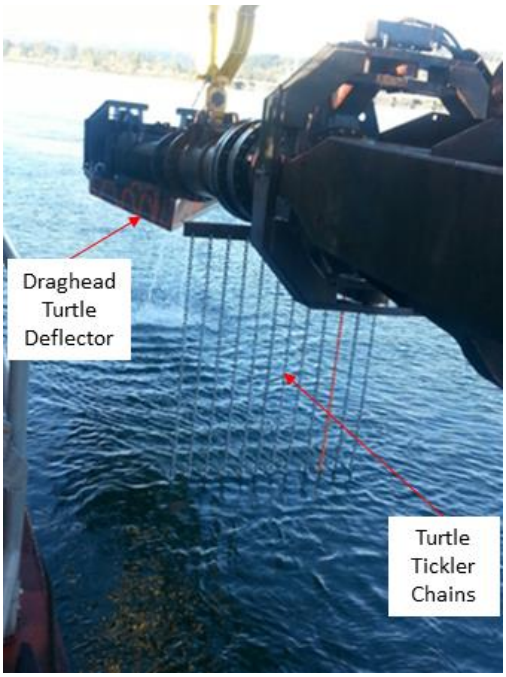

Figure 5. Draghead turtle deflector and TTC on the ESSAYONS port dragarm (looking aft).

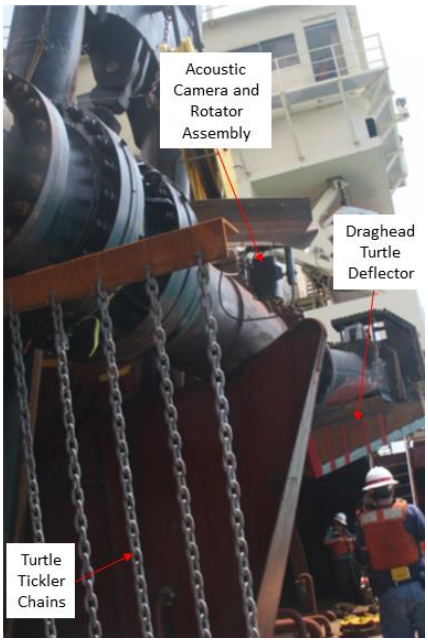

Figure 6. Acoustic camera with pan/tilt rotator assembly mounted on port dragarm between TTC and draghead turtle deflector (looking aft).

FIELD DEPLOYMENT RESULTS AND DISCUSSION

The tests conducted at Kalaeloa Barber's Point on 24 March 2016 consisted of observing the TTC and draghead during normal dredging operations with the real-time monitoring and video recording systems during the first two hours of dredging (between 1400 and 1600-hours). The GoPro cameras required the data to be downloaded after the dragarm was retrieved on deck. A few minutes into the first test, the camera equipment became submerged in the predominantly fine-grained (muddy) shoaling material because the bottom was so unconsolidated that the draghead easily penetrated the harbor bottom. Immediately after the live camera feed went black, the dragtender was instructed to pull the dragarm up to clean and inspect the camera systems. No damage was found to any of the equipment. The risk of damaging or losing the expensive acoustic camera system in the mud became a paramount concern in the following tests and draghead depth relative to bottom elevation was monitored closely.

Water visibility in the harbor at Kalaeloa Barbers Point limited data quality collected by the GoPro and high definition cameras. Even prior to the dragheads entering the water, the bottom sediments were already being re-suspended by the propeller wash from the maneuvering ESSAYONS. The initial real-time images from the high-definition camera (and those from the GoPros post retrieval) showed the chains and seafloor. However, the image quality quickly degraded once the dragheads were dragged through the bottom sediment and the ESSAYONS' propellers and bow-thrusters were rotated - substantially increasing the suspended sediment concentrations due to resuspension. The GoPro mounted to the bottom of the turning gland produced the best video early in the test, when the top of the chains were immediately above the bed sediment (Figure 7).

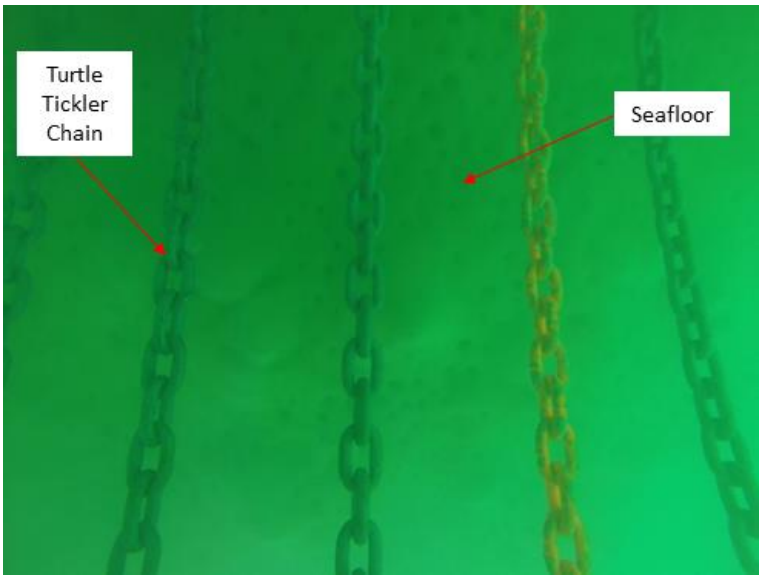

Figure 7. Image of the chain array from the GoPro camera on the bottom of the dragarm turning gland.

Since the acoustic camera was on a pan and tilt mount, it could be adjusted remotely while dredging was in progress to view either the TTC or draghead turtle deflector. Even with the turbid water and mechanical vibrations during dredging, the acoustic camera was able to provide relatively clear images of the TTC, draghead turtle deflector, seafloor, and sediment movement. When the TTC were suspended in the water column as the dredge moved, the acoustic camera images clearly showed the individual chains hanging down from the dragarm and not becoming entangled. Figure 8 shows the TTC immediately suspended off the harbor bottom. Due to the acoustic camera's grazing angle and distance to the chains, it was not possible to view the entire $3\,m$ lengths of all the chains simultaneously. The rotator assembly was required to tilt the acoustic camera to scan from the top of the chain mount down to the chain ends.

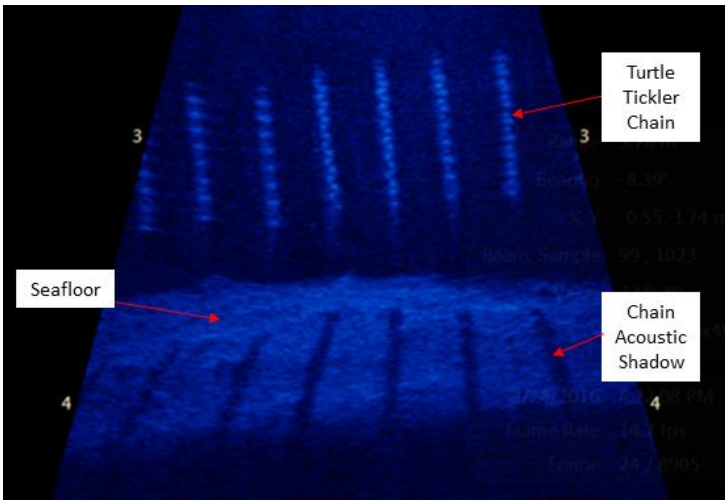

Figure 8. Acoustic camera image of TTC free-streaming in water column above the harbor bottom.

When the draghead was on bottom, the TTC maintained contact with the seafloor, did not entangle, and maintained a relatively constant separation distance between individual chain lengths (see Figure 9). It is important to note that the video (as opposed to still images taken from the video shown here) provides a more complete interpretation of what is being viewed.

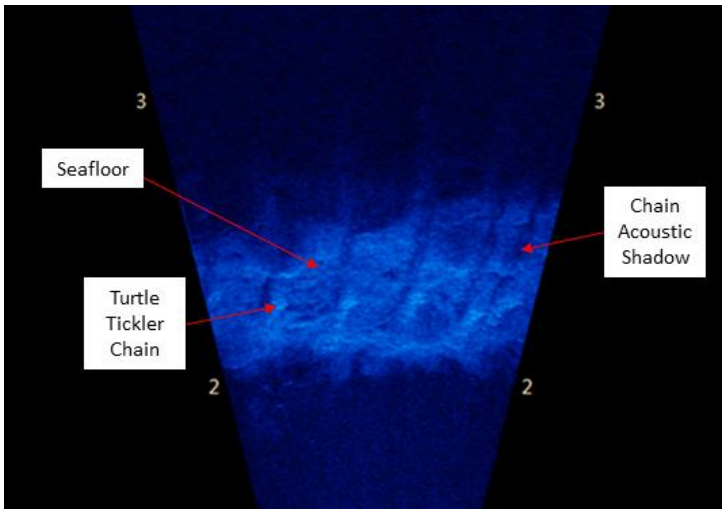

Figure 9. Acoustic camera image of TTC dragging on harbor bottom.

As the principle objective of the field deployment was to assess the performance of the TTC, the acoustic camera was mounted and positioned to optimize the view of the TTC. Fortunately, it was also possible to view the forward end of the draghead and turtle deflector due to the ability to adjust the acoustic camera with the pan and tilt mount Figure 10 shows these features while the dragarm was suspended in the water column. Figure 11 shows the draghead on the seafloor - the sediment wave can be clearly seen building up in front of the draghead as it is plowed through the sediment. These acoustic camera images clearly confirm that the draghead deflector was positioned correctly to create the sediment wave forward of the draghead necessary to induce sea turtles to move away.

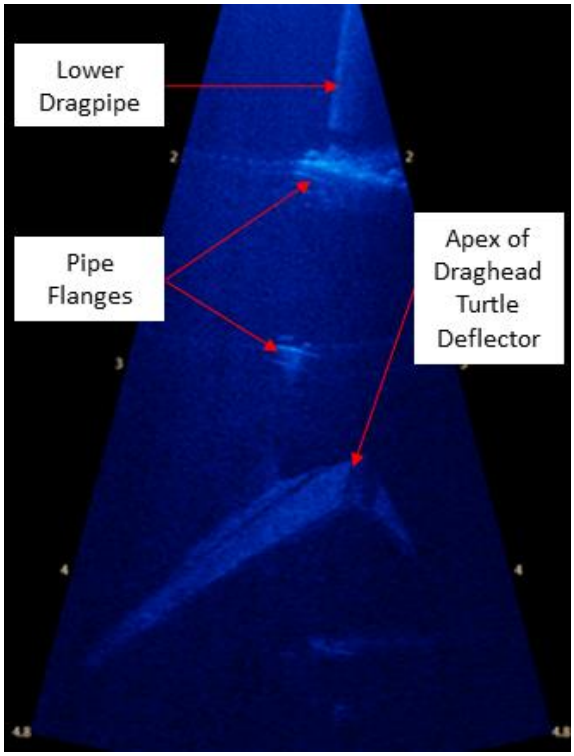

Figure 10. Acoustic camera image of the draghead with turtle deflector suspended in the water column.

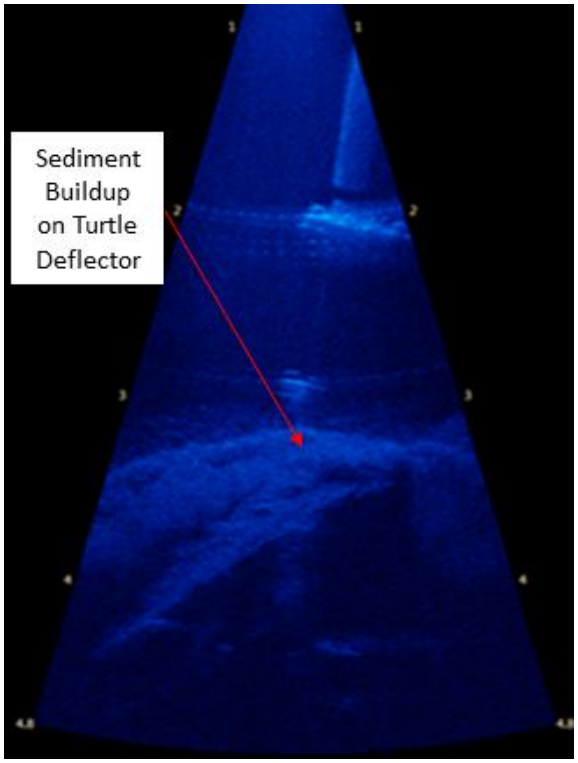

Figure 11. Acoustic camera image of the draghead in mud with sediment wave building up on turtle deflector.

CONCLUSIONS

Laboratory and field efforts presented herein have successfully highlighted the applications of high resolution acoustic cameras. The laboratory experiment made use of an acoustic camera to measure the fall velocity of three different particles: 5 mm Styrene, 1 mm Cellulose Acetate, and 0.5 mm Polymethyl Methacrylate (PMMA) spheres. The measured terminal fall velocity of the particles showed excellent agreement with the theoretical terminal fall velocity, with a percent error of 1 % or less (relative to the theoretical terminal fall velocity) for all particles tested. Additionally, the qualitative behavior of the particle settling trajectories was as expected from intuition. This indicates acoustic cameras can accurately quantify particle motion for particles greater than 0.5 mm, and is a promising step in moving towards the use of acoustic cameras to quantify two-dimensional velocity fields.

To test the operating capabilities of the acoustic camera in highly dynamic and turbid dredging environments, an acoustic camera was attached via a pan/tilt rotator assembly to the port dragarm of the USACE dredge ESSAYONS. Optical cameras were deployed simultaneously to compare the optical images to those of the acoustic camera. Both types of cameras monitored the performance of Turtle Tickler Chains (TTC) and the acoustic camera additionally monitored the interaction of the draghead and turtle deflector with the sediment. The TTC was observed to maintain quasi-steady spacing, maintain contact with the bed, and remain un-entangled for the duration of the test as required. Poor visibility due to suspended sediments from the dredge's propeller and bow thrusters reduced the image quality of the optical cameras long before the dragheads began dredging. Optical image quality rapidly degraded after the dragheads were dragged along the bottom, to such an extent that the acoustic camera was the only viable instrument to monitor the TTC.

In summary, the results presented in this study indicate that acoustic cameras are able to quantify the motion of sub-millimeter inertial particles under laboratory conditions, as well as operate from dynamic platforms in extremely turbid, low visibility environments commonly found near dredging operations. Therefore, acoustic cameras are a promising technology for monitoring dredging operations.

REFERENCES

Hedrick, T. (2008). "Software Techniques for Two- and Three-Dimensional Kinematic Measurements of Biological and Biomimetic Systems." *Bioinspiration and Biomimetics*, 3.3, 34001.

Kundu, P.K. and Cohen, I.M. (2008). *Fluid Mechanics (4th ed.).* Elsevier Academic Press, Amsterdam, The Netherlands.

Munson, B.R., Young, D.F., and Okiishi, T.H. (2002). *Fundamentals of Fluid Motion*. John Wiley and Sons, Hoboken, New Jersey.

National Marine Fisheries Service. (2016). "Endangered Species Act – Section 7 Consultation Biological Opinion and Conference Opinion," National Marine Fisheries Service-Pacific Islands Region-Protected Resources Division, NMFS File No. PIR-2014-9570, PIRO Reference No. I-PI-15-1218-AG, 3 Mar 2016. 81p.

Tropea, C., Yarin, A., and Foss, J.F. (2007). *Springer Handbook of Experimental Fluid Mechanics*. Springer, Berlin, Germany.

Urick, R.J. (1983) *Principles of Underwater Sound (3rd ed.).* McGraw-Hill, New York, New York.

Van Veen, B.D. and Buckley K.M. (1988) "Beamforming: A Versatile Approach to Spatial Filtering." *IEEE asp magazine*, 5(2), 4-24.

CITATION

Young, D.L., McFall, B.C., Welp, T.L., and Dickerson, D.D. "Use of Acoustic Cameras in Dredging Research." *Proceedings of the Twenty-Second World Dredging Congress, WODCON XXII, Vancouver, BC*, Canada, June 26-29, 2017.

ACKNOWLEDGEMENTS

This study was funded through the USACE Dredging Operations and Environmental Research (DOER) program. The cooperation of the crew of the USACE dredge ESSAYONS is graciously acknowledged. The contents of this paper are not to be used for advertising, publication, or promotional purposes. Citation of trade names does not constitute an official endorsement or approval of the use of such commercial products.